

A Novel Chimeric Poxvirus Encoding hNIS Is Tumor-Tropic, Imageable, and Synergistic with Radioiodine to Sustain Colon Cancer Regression

Susanne G. Warner,^{1,2} Sang-In Kim,¹ Shyambabu Chaurasiya,¹ Michael P. O'Leary,¹ Jianming Lu,¹ Venkatesh Sivanandam,¹ Yanghee Woo,¹ Nanhai G. Chen,^{1,2} and Yuman Fong^{1,2}

¹Department of Surgery, Division of Surgical Oncology, City of Hope National Medical Center, Duarte, CA 91010, USA; ²Center for Gene Therapy, Beckman Research Institute, City of Hope National Medical Center, Duarte, CA 91010, USA

Colon cancer has a high rate of recurrence even with good response to modern therapies. Novel curative adjuncts are needed. Oncolytic viral therapy has shown preclinical promise against colon cancer but lacks robust efficacy in clinical trials and raises regulatory concerns without real-time tracking of viral replication. Novel potent vectors are needed with adjunctive features to enhance clinical efficacy. We have thus used homologous recombination and high-throughput screening to create a novel chimeric poxvirus encoding a human sodium iodide symporter (hNIS) at a redundant *tk* locus. The resulting virus (CF33-hNIS) consistently expresses hNIS and demonstrates replication efficiency and immunogenic cell death in colon cancer cells *in vitro*. Tumor-specific CF33-hNIS efficacy against colon cancer results in tumor regression *in vivo* in colon cancer xenograft models. Early expression of hNIS by infected cells makes viral replication reliably imageable via positron emission tomography (PET) of I-124 uptake. The intensity of I-124 uptake mirrors viral replication and tumor regression. Finally, systemic delivery of radiotherapeutic I-131 isotope following CF33-hNIS infection of colon cancer xenografts enhances and sustains tumor regression compared with virus treatment alone in HCT116 xenografts, demonstrating synergy of oncolytic viral therapy with radioablation *in vivo*.

INTRODUCTION

Colorectal cancer is the third leading cause of cancer death in the United States.¹ Improvements in treatment and screening have contributed to an increase in overall survival, but patients presenting with distant metastases still have a dismal survival, even with modern chemotherapies.^{2,3} Therefore, novel therapies are needed. Oncolytic viruses are naturally occurring or genetically modified viruses that infect, replicate in, and kill cancer cells, leaving healthy cells unharmed. Viruses can also be engineered to engage the immune system and enhance local and systemic anti-tumor immune reactions.⁴ Despite preclinical promise, challenges related to potency, track-ability of viral replication, and durable clinical responses have slowed the progression of oncolytic viruses to standard cancer therapy.^{5,6} The first obstacle is the relative lack of potency of existing viral vectors. In particular, the hurdle of lower potency means more viral particles

are required per dose, creating excessive expense. Moreover, higher doses required to achieve therapeutic benefit can yield substantial toxicities and prohibit effective dosing strategies. For instance, clinical trial results confirm that oncolytic viral therapy using poxvirus-based and other viral vectors is safe and demonstrates clear biologic activity against cancers refractory to traditional adjuvant therapies.^{7,8} However, a current poxvirus in clinical trials requires three doses of 10⁹ plaque-forming units (PFU) of virus, making therapy extremely expensive and making toxicity more likely.⁹ Thus, more potent, tumor-selective viruses capable of more efficient viral replication are needed. This project aimed to characterize a novel chimeric poxvirus (CF33-hNIS) that we created via an innovative recombination technique. This virus is potent, replicates efficiently, and allows for additional deliverables in the form of noninvasive imaging and therapeutic synergy.

To noninvasively track viral replication in real time and facilitate synergy with therapeutic radioisotopes, CF33-hNIS has been engineered to encode a human sodium iodide symporter (hNIS). Our group and others have established that viral infection and proliferation can be noninvasively imaged *in vivo* using a number of different reporter genes.^{10,11} hNIS is able to facilitate both imaging and synergistic cell kill via radioisotope uptake.^{12,13} Thus, CF33-hNIS replication and efficacy can be both tracked (via positron emission tomography [PET] or single-photon emission computed tomography [SPECT] imaging) and enhanced (via addition of radioisotopes, which can ablate cells surrounding an infected cell that takes in the isotope). Clinically, this means that one day a patient could receive a dose of virus, be imaged several days later to identify known and unknown sites of tumor via viral replication, and then receive adjunctive radioisotope that could augment cytotoxic effects of already replicating oncolytic virus.

Received 26 March 2019; accepted 4 April 2019;
<https://doi.org/10.1016/j.omto.2019.04.001>

Correspondence: Susanne G. Warner, MD, Department of Surgery, Division of Surgical Oncology, City of Hope National Medical Center, 1500 E. Duarte Road, MOB 1002B, Duarte, CA 91010, USA.

E-mail: suwarner@coh.org



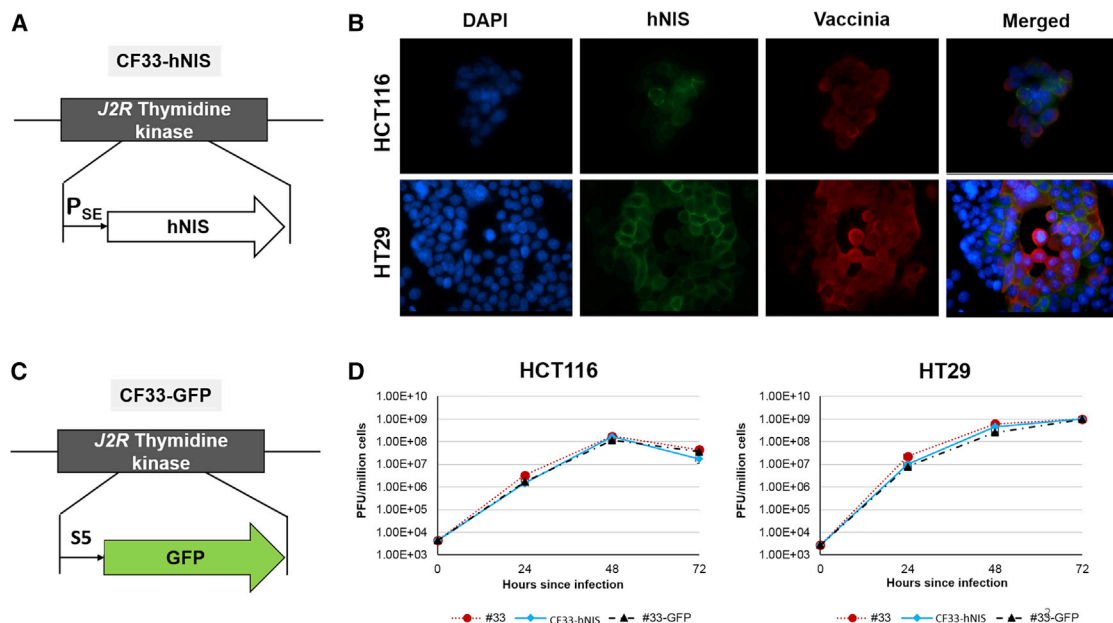


Figure 1. Chimeric Orthopoxvirus CF33 Expressing hNIS

(A) Schematic represents *tk* locus insertion of hNIS at *tk* locus under the control of the synthetic early (SE) promoter. (B) Immunofluorescence demonstrates co-staining with vaccinia (red) and hNIS (green) at 24 h post-infection with CF33-hNIS at MOI 0.01 in HCT116 (upper panel) and HT29 (lower panel) cells magnified at $\times 60$. DAPI (blue) was used for nuclei staining. (C) Schema depicting insertion of GFP on *tk* locus, instead of hNIS, to generate CF33-GFP. (D) Viral replication in HCT116 and HT29 at an MOI of 0.01. Bars indicate SD. hNIS, human sodium iodide symporter; PSE, synthetic early promoter.

This study sought to characterize the efficacy of CF33-hNIS against colon cancer *in vitro* and *in vivo*, and to evaluate its capability to induce *in vivo* radioisotope uptake. This study further investigates cell death patterns of CF33-hNIS against preclinical colorectal cancer models and the use of radioisotopes for synergistic tumor destruction *in vitro* and *in vivo*. We hypothesized that CF33-hNIS is tumorigenic, and that viral replication is imageable in real time. We further hypothesized that viral infection would facilitate synergy with therapeutic radioisotopes, and that cell death from viral infection would occur via mechanisms commonly attributed to poxvirus infection.

RESULTS

CF33-hNIS Infects, Replicates in, and Kills Colon Cancer Cells

Chimerization and high-throughput analysis yielded a successful chimeric orthopoxvirus candidate that resulted in superior cell killing and viral replication when compared with parental strains, as previously reported.^{14–16} Insertion of hNIS at the *tk* locus (Figure 1A) resulted in consistent hNIS expression, which can be observed on the surface of cells infected with CF33-hNIS that stain positive for vaccinia (Figure 1B). We also generated a version of CF33 expressing GFP (CF33-GFP; Figure 1C) for our studies. Deletion of *tk* locus did not appear to attenuate viral replication efficacy *in vitro*, regardless of inserted reporter gene (Figures 1C and 1D).

CF33-hNIS demonstrated anti-tumor efficacy in a dose-dependent manner against HT29 and HCT116 cells (Figure 2). At 120 h post-infection, at MOI of 1.0, both HCT116 (Figure 2A) and HT29 cells

(Figure 2B) experienced near-complete cell death relative to control. At lower concentrations, less than 20% of cells were alive relative to control at the same 120-h time point.

CF33-hNIS Induces Cancer Cell Death via Immunogenic Cell Death Pathways

In order to identify mechanisms of cell death stimulated upon infection with CF33-hNIS, we examined a wide array of cell death assays. First, CF33-hNIS-infected cells were assayed for phosphatidyl serine exposure with Annexin V and stained for active caspase-3, as well as for incorporation of propidium iodide (PI), at 18 and 48 h post-infection and compared with uninfected cells (Figure 3A). At 18 and 48 h, whereas the majority of HT29 cells were PI-positive, very few HT29 cells stained positive for caspase-3 and Annexin V, which are standard markers of apoptosis (Figure 3A). Similarly, in HCT116 cells, 46% of infected cells were positive for PI staining at 18 h, and over 80% of infected cells were PI-positive at 48 h, but minimal to no caspase or Annexin staining was seen (Figure 3A).

The absence of apoptosis hallmarks was confirmed with the terminal deoxynucleotidyl transferase dUTP nick-end labeling (TUNEL) assay, which demonstrates apoptosis-associated DNA degradation (Figure S1). TUNEL assay results demonstrated little to no evidence of DNA nicking in infected cells with virtually no difference between infected cells and controls, again demonstrating deviation from traditional apoptosis, pointing to caspase-independent cell death pathways, and suggesting the involvement of necroptosis.

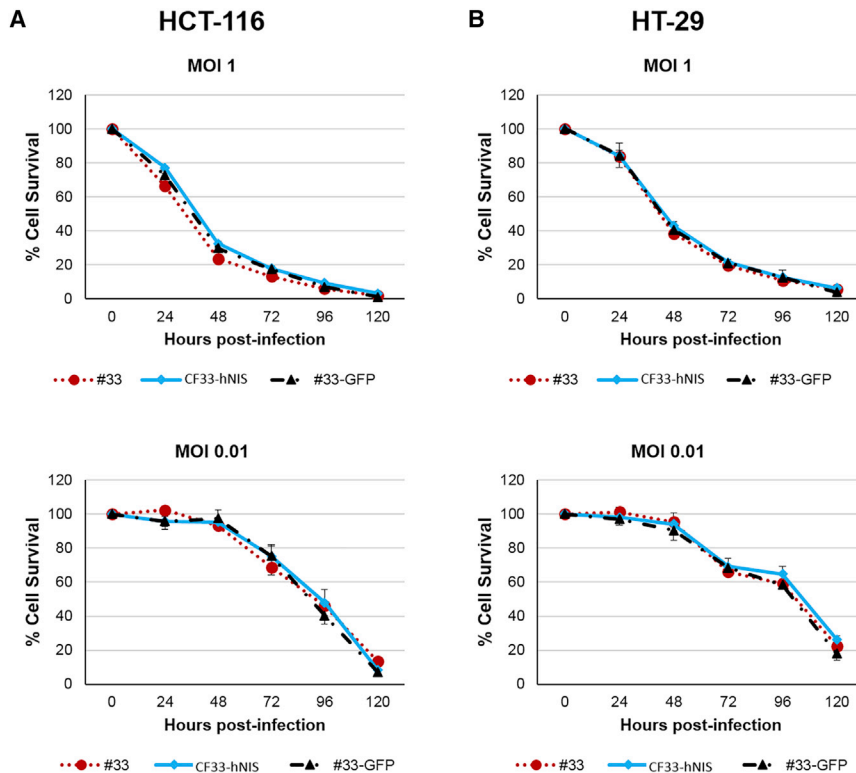


Figure 2. CF33-hNIS Kills Colon Cancer in a Dose-Dependent Manner with Viral Efficacy Unaltered by *tk* Deletion

(A) Cytotoxicity of CF33-hNIS against HCT116 as compared with CF33 backbone virus (#33), CF33-GFP, which shares the same backbone of CF33-hNIS virus but has GFP inserted at *tk* locus (#33-GFP). (B) Cytotoxicity against HT29. For cytotoxicity experiments, cells were infected at MOI 1 and MOI 0.01. Bars indicate SD. NIS, sodium iodide symporter.

with established HT29 and HCT116 flank xenografts that had been treated with either intratumoral PBS, CF33-luciferase (another described CF33 derivative with deleted *tk* locus),¹⁴ or CF33-hNIS. A representative set of images in mice bearing HCT116 xenografts is shown in Figure 4A. In Figure 4B, we show serial images taken over several days after the initial viral injection and demonstrating an increase in signal on day 15 (Figure 4B, middle panel) compared with day 7 (Figure 4B, left panel). This suggests an increase in viral replication and accumulation in the tumor, which has been confirmed in models correlative with viral titer using similar CF33-luciferase.¹⁵ Non-injected contra-

lateral tumors also demonstrated hNIS expression and I-124 uptake commensurate with viral infection (Figure 4B, right panel, day 22). Expected basal hNIS expression also resulted in I-124 uptake in thyroid, stomach, and isotope excretion in the bladder in addition to tumor tissues. No I-124 tumor uptake was noted in PBS or CF33-luciferase control mice.

CF33-hNIS Induces Tumor Regression in HCT116 Human Colon Cancer Xenografts

We next examined the effect of CF33-hNIS on tumor growth. HT29- and HCT116-induced flank xenografts were implanted into athymic nude female mice. When tumors reached an average volume of 150 mm³, they received intratumoral PBS or CF33-hNIS injections at 1×10^5 PFU. CF33-hNIS caused tumor growth abrogation and later regression in animals with HCT116-derived xenografts that was noticeable around days 10–15 and that was sustained from then up to the end of the study period (day 55). CF33-hNIS also promoted tumor regression and growth abrogation of HT29-derived tumors in some mice, although the observed aggregate effect was not statistically significant (Figure 5B). More specifically, heterogeneity of HT29-based xenograft formation does adversely affect our ability to draw conclusions regarding viral efficacy. For example, in the treatment group, one outlier that did not appear to experience uniform tumor infection grew quite large. In the same HT29 group, there was a PBS control mouse that had very little tumor growth, thus bringing these curves closer together (Figure 5). In repeat HT29 experiments, heterogeneity of xenograft formation resulted in similar

Finally, mechanisms of immunogenic cell death (ICD) were examined. ICD is distinctively accompanied by the translocation of calreticulin from the endoplasmic reticulum onto the outer leaflet of the plasma membrane, both by secretion of ATP and release of HMGB1 into supernatant.¹⁷

Upon CF33-hNIS infection, we observed calreticulin-positive staining in 30% of infected HT29 cells versus 13% in controls (Figure 3B). This effect was also seen in HCT116 cells (20% of infected cells versus 10% in uninfected control). An increase in supernatant secretion of ATP was also seen (Figure 3C), wherein we observed greater than 30-fold increase of extracellular ATP between infected and non-infected HT29 cells (Figure 3C, left panel), and a greater than 10-fold increase in infected HCT116 cells (Figure 3C, right panel). Lastly, we observed a substantial increase in HMGB1 in the supernatants of infected HT29 and HCT116 cells compared with uninfected controls (Figure 3D). These findings cumulatively identify cell death mechanisms most consistent with ICD, as indicated by the markers that have been implicated in immunogenicity following oncolytic virus-induced cellular destruction.

PET/CT I-124 Imaging of CF33-hNIS-Infected Tumor Cells Demonstrates Functional hNIS Expression *In Vivo* and Confirms Tumor Specificity of Virus

We wanted to determine whether the expression of hNIS induced by viral infection could allow us to image infected tumors in real time. Using PET/computed tomography (CT), we imaged nude mice

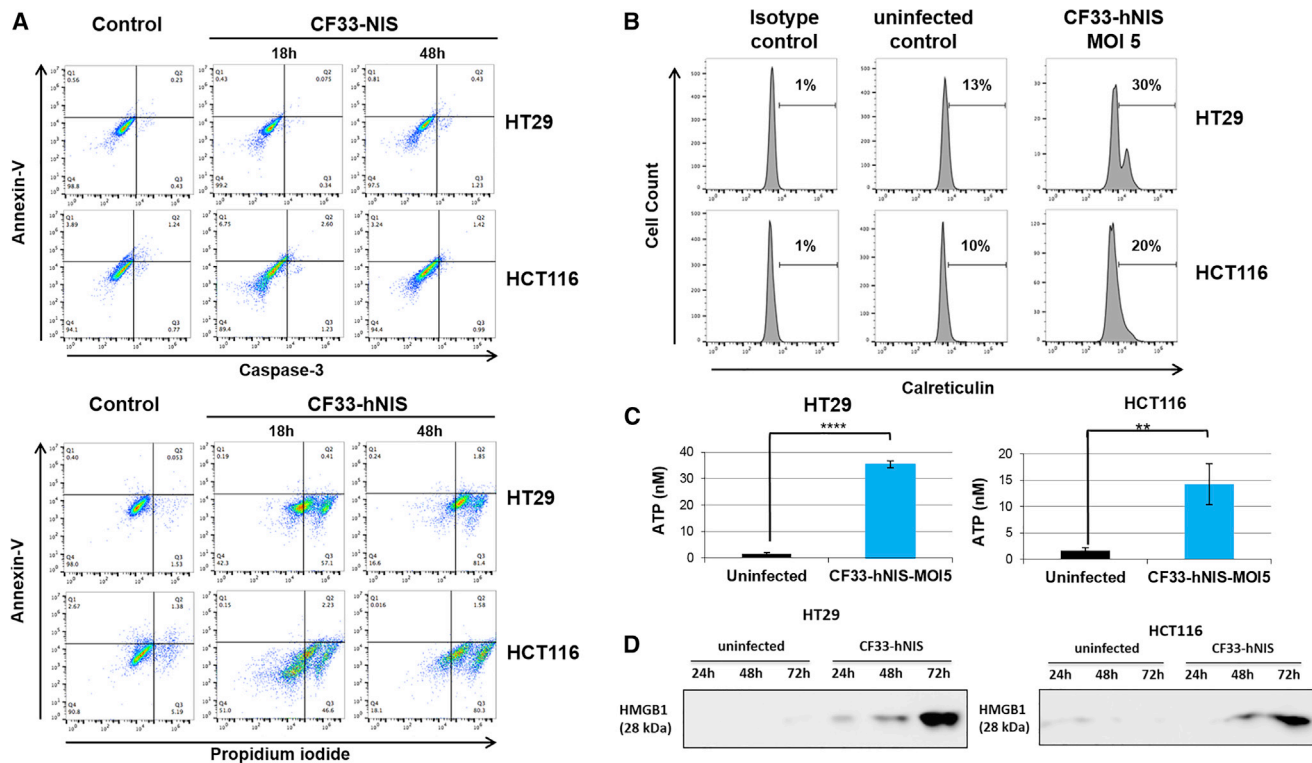


Figure 3. CF33-hNIS Induces Caspase-Independent Immunogenic Cell Death

(A) Cells were infected at MOI 5. At 18 and 48 h post-infection, cells were stained for Annexin V, caspase-3, and propidium iodide, fixed, and analyzed by flow cytometry. (B) For calreticulin detection, cells were infected with CF33 or CF33-hNIS (MOI 5) for 16 h. 1×10^6 cells were resuspended in PBS containing 2% FBS and stained with antibody against calreticulin or an isotype control antibody (EPR3924; Abcam). After staining, cells were analyzed by flow cytometry. (C) Cells were left uninfected or received CF33-hNIS (MOI 5). After 16 h of incubation, supernatants were collected and ATP was measured using ATP determination kit. Statistical significance was determined by Student's *t* test; ***p* < 0.01, *****p* < 0.0001. (D) Cells were infected with CF33-hNIS (MOI 5), and supernatants were collected at 24, 48, and 72 h post-infection. Supernatants were concentrated using centrifugal filters. Proteins in the supernatants were resolved by SDS-PAGE, and HMGB1 was detected by western blot analysis. Representative western blots are shown. CRT, calreticulin; HMGB1, high-mobility group box 1 protein; NIS, sodium iodide symporter.

outlier situations. Nevertheless, there were observed mice in all HT29 treatment groups with tumor regression. HCT116-derived xenografts demonstrated more uniform tumor formation and more uniform tumor regression following viral infection (Figure 5). Immunohistochemical examination of tumors demonstrates abrogation of tumor cell division in virus-treated groups with substantial inflammatory infiltrate around tumor cells that is not present in untreated xenografts (Figure 5). Finally, upon immunohistochemical analysis at 10 days following viral injection, only tumor sections demonstrated positive staining for virus (Figure S2).

CF33-hNIS Infection Is Synergistic with I-131 Radioisotope and Induces Sustained Tumor Growth Abrogation in HCT116 Xenografts

To explore whether expression of hNIS by infected tumor cells could lead to synergistic tumor destruction using CF33-hNIS in combination with I-131, mice bearing bilateral flank xenografts established with HCT116 or HT29 colorectal cancer cells were treated with unilateral intra-tumoral injections with: (1) PBS alone, (2) I-131 alone, (3) CF33-hNIS alone, or (4) CF33-hNIS + I-131. It should be noted

that in order to adequately evaluate synergy, a lower dose of virus (1×10^4 PFU) was used than was employed in tumor regression experiments (1×10^5 PFU). Mice treated with PBS or I-131 alone showed unrestrained tumor growth and had to be euthanized by day 30 upon reaching predetermined tumor size limits (Figures 6A and 6B). Single treatment with intravenous (i.v.) I-131 did promote some reduction in tumor growth compared with control in HCT116-derived tumors (Figure 6A), but not in HT29-derived tumors (Figure 6B). Although intratumoral CF33-hNIS treatment alone showed expected tumor growth abrogation (Figure 5), the combination of i.v. I-131 plus intratumoral CF33-hNIS demonstrated superior tumor growth abrogation and regression in HCT116 xenografts (Figure 6A). Importantly, this observed tumor regression was sustained over time during the study period (Figure 6A). Immunohistochemical examination of tumors demonstrates an absence of tumor cells in combination-treated tumors along with a sizable inflammatory infiltrate (Figure 6B). In the HT29 xenografts group, statistical significance was not achieved between virus alone and virus plus I-131 groups prior to euthanasia, which was required secondary to growth of non-injected tumors on contralateral flanks.

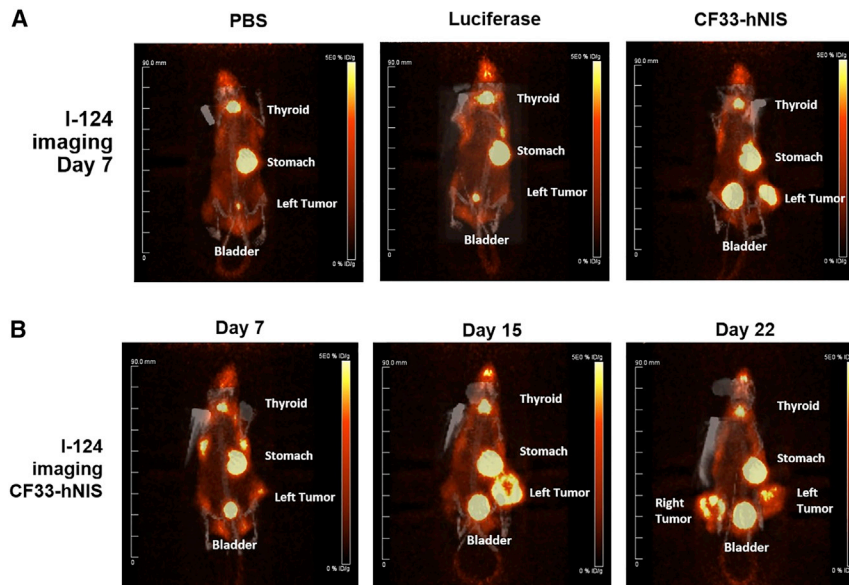


Figure 4. I-124 Imaging of 33-NIS-Infected Tumor Cells *In Vivo*

CF33-hNIS is tropic for tumor cells, and CF33-hNIS-infected tumor cells take up I-124 and are thus imageable using PET/CT. HCT116 and HT29-derived flank xenografts were implanted in nude mice using 3×10^6 cells per tumor. When tumor volume reached a predetermined 150 mm^3 , mice received intratumoral (i.t.) injections of PBS, CF33-FLuc, or CF33-hNIS at a dose of 10^4 PFU. (A) Comparisons of PET/CT images on day 7 across treatment and control groups 2 h following i.v. injection of $200 \mu\text{Ci}$ of I-124. (B) Images of a single mouse over time. Note I-124 uptake in right-sided tumor on day 22 despite injection of only left-sided tumor. NIS, sodium iodide symporter; PFU, plaque-forming units.

Our present study shows synergy between CF33-hNIS and I-131, which underscores the importance of treatment strategies to augment and sustain viral efficacy as we move forward translating these findings to clinical use. Several groups

DISCUSSION

This study reports that our novel chimeric orthopoxvirus CF33-hNIS is able to infect, replicate in, and kill colon cancer cells, and induce sustained regression of tumor *in vivo*. Herein, we further confirm our hypothesis that the addition of hNIS to the viral genome results in infected cancer cell expression of functional hNIS that in turn allows for uptake of radioisotope. This enables real-time imaging of virally infected cells via PET imaging of I-124 uptake along with synergy with therapeutic radioiodine (I-131), which facilitates ablation of surrounding cells. The *in vivo* findings of tumor regression occur at doses 1–4 logs lower than those used by other groups with vaccinia-based vectors in similar experiments.^{18,19} Moreover, this work demonstrates that the synergistic addition of radioiodine ablation to oncolytic viral infection sustains oncolytic virus-induced tumor regression. Thus, an oncolytic virus (OV) carrying hNIS permits local radiotherapy by eliciting a high concentration of radioisotope, which may be used clinically to decrease undesired side effects and enhance viral efficacy at lower, less toxic, less expensive doses. As a well-known theranostic tool, it also holds promise for direct noninvasive scintigraphy and PET imaging to allow both evaluation of viral biodistribution and dosimetric calculations as a prerequisite for planning therapy studies with higher doses of radioisotopes like Re-188 and I-131.^{20–24}

This project further examines cell death patterns of our novel chimeric vector and demonstrates evidence of robust ICD via caspase-independent pathways consistent with the vector's parent orthopoxviruses.^{25,26} This has important implications for clinical translation as we move forward, given viral potential to activate otherwise immunosuppressive microenvironments, leading to an increase in the recruitment of immune cells to tumors and promotion of an anti-tumor immune response. Experiments outside of the scope of this work are planned to evaluate the relationship between cell death induced by this vector and anti-tumor immunity.

have demonstrated that the radiotracer uptake resulting from virally induced hNIS expression occurs in a dose-dependent manner regardless of radiotracer and modality used (I-124PET, $^{99\text{m}}\text{TcO}_4$ SPECT, or I-123 scintigraphy). Herein, we have demonstrated robust radioiodine uptake at viral doses 1–2 logs lower than previously reported, again speaking to the enhanced potency of CF33-hNIS.^{11,27–29} Our group and others have previously demonstrated that PET signal pattern also correlates with anti-tumor response to viral therapy.¹² We have shown this with an earlier generation of this novel vector encoding a luciferase reporter gene and bioluminescent imaging,¹⁵ and have herein confirmed this principle using I-124 PET imaging. More extensive experiments are planned to confirm dosimetric delivery of radioisotope and viral tumor titration at each point of imaging.

This work demonstrates that I-131 synergizes with CF33-hNIS to prolong tumoricidal oncolytic effects of CF33-hNIS. Using doses of 2.5 and 2.0 mCi of I-131 along with low doses (1×10^4 PFU) of virus, we have demonstrated enhanced potency over previous experiments.^{13,30} Previous studies from our group have shown radiotracer (I-124) uptake of engineered vaccinia virus GLV-1h153 in orthotopic triple-negative breast tumors in athymic nude mice at doses of 1×10^7 PFU and have demonstrated synergy with I-131 at dose of 1×10^6 PFU for triple-negative breast cancer and at 1×10^5 PFU for pancreas cancer-derived xenografts, but at both of these doses of virus, little to no viral effect was seen on tumor treatment.^{13,31} We were pleased that imageable uptake and viral-induced tumoricidal activity occurred robustly with CF33-hNIS at doses of just 1×10^4 PFU, suggesting enhanced potency of our virus over prior constructs. Moreover, synergy of CF33-hNIS with 2.0–2.5 mCi of i.v. I-131 is noted at similar i.v. doses as previously used with triple-negative breast models (5 mCi) and pancreas models, which demonstrated dose-dependent synergy at 1.0 and 2.5 mCi doses along with a vaccinia-based virus. Of note, Mansfield et al.³² have employed intraperitoneal dosing of

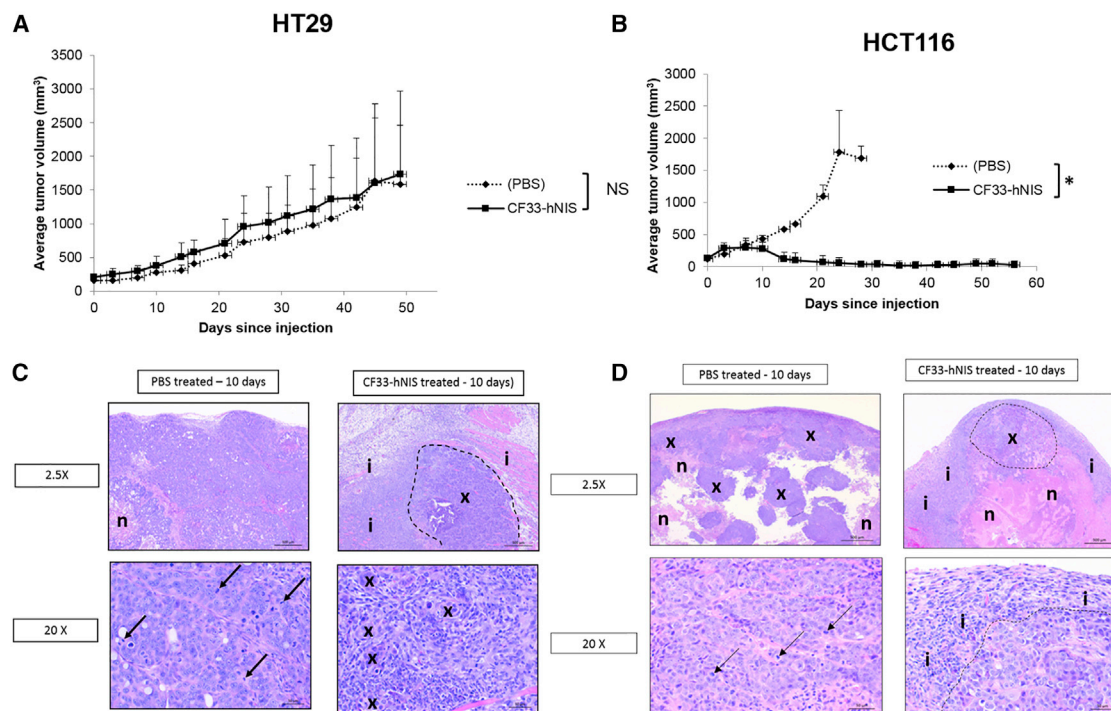


Figure 5. CF33-hNIS Kills Human Colon Cancer HCT116 Xenografts and Demonstrates Substantial Tumor Cell Damage in HT29 Xenografts

Flank xenografts were created in nude mice with 5×10^6 cells. Tumors were injected with 1×10^5 PFU of CF33-NIS when they reached average volume of 150 mm^3 . (A and B) Results from HT29 (A) and HCT116 (B) xenografts are shown with virus (solid line) versus sham infection (dashed line). $n =$ at least 4 per treatment group. (C) Representative immunohistochemical examination of intra-tumorally treated HT29 tumors 10 days following injection demonstrates abrogated cell division and substantial inflammation relative to controls: the tumor from the PBS-treated mouse (PBS-treated; left panels) is composed almost entirely of xenograft cells and contains only a small area of necrosis (n). Mitotic figures (lower left; arrows) are common in xenograft cells, and little, if any, inflammatory cell infiltrate is present. The xenograft tumor from CF33-hNIS-treated mouse (right panels) has an area of xenograft cells (top right; circled and labeled x) that is surrounded by a thick zone of inflammation (i). The photograph at bottom right shows small clusters of xenograft cells (x) surrounded by an abundant infiltrate of mononuclear (lymphocytes and macrophages) inflammatory cells. Mitotic figures are uncommon in xenograft cells. H&E stain is shown. (D) Representative immunohistochemical examination of intra-tumorally treated HCT116 tumors 10 days following injection demonstrates abrogated cell division and substantial inflammation relative to controls: the tumor from the PBS-treated mouse (left panels) has abundant areas composed of xenograft cells (x) intermixed with areas of necrosis (n). The empty spaces in the photograph (top left) are likely areas of liquefied, necrotic cell debris that were lost during tissue collection and processing. Little, if any, inflammatory cell infiltrate is present around or within this tumor. Mitotic figures are common in xenograft cells (lower left; arrows). The xenograft tumor from mouse 128_CF33-hNIS (right panels) has only a small area composed of xenograft cells (top right; circled and labeled x), large areas of necrosis (n), and thick, surrounding zone of inflammatory cell infiltrate (i). The photograph at bottom right shows the xenograft cells (below and right of dashed line) and the adjacent thick zone comprised of mononuclear (lymphocytes and macrophages) inflammatory cells (i). Xenograft cells in this tumor are smaller, and mitotic figures are uncommon. H&E stain is shown. NIS, sodium iodide symporter; NS, non-significant; PFU, plaque-forming units. * $p < 0.05$.

I-131 at 1 mCi and seen synergistic effects. We have also seen synergy at markedly low intraperitoneal (i.p.) dosing compared with i.v. (data not shown) and are currently investigating these observations.

Cell death induced by replication of oncolytic viruses varies widely among vectors and cell types. Although poxvirus-induced cell death does not fit perfectly into any of the traditionally described cell death pathways like apoptosis, necrosis, or autophagy,⁷ there is growing evidence that most vaccinia-infected cells die via caspase-independent programmed necrosis, also known as necroptosis. Importantly, poxvirus-induced cell death pathway is also immunogenic.^{15,33–35} Indeed, many vectors are now shown to induce ICD, which is thought to enhance viral capability to affect anti-tumor immunity. We have recently demonstrated that chimerization of multiple orthopoxviruses

yields a more potent virus than parental strains when tested against the National Cancer Institute-60 (NCI-60) panel of cell lines.¹⁵

Interestingly, previous studies have demonstrated that vascular shutdown resulting from viral infection, such as that seen with vesicular stomatitis virus (VSV) and vaccinia virus in subcutaneous colon cancer models, can limit delivery of radiotracers and inaccurately downplay tracking of viral infection that may be occurring beyond collapsed blood vessels.³⁶ We did note decreased uptake of I-124 commensurate with decreased viral replication as tumor cell destruction occurred and virus dissipated. However, we saw no evidence on immunohistochemical examination that rather than tumor cell death, a zone of vascular shutdown and necrosis limited virally infected cells taking up radiotracer. Further studies are planned with CF33-hNIS to

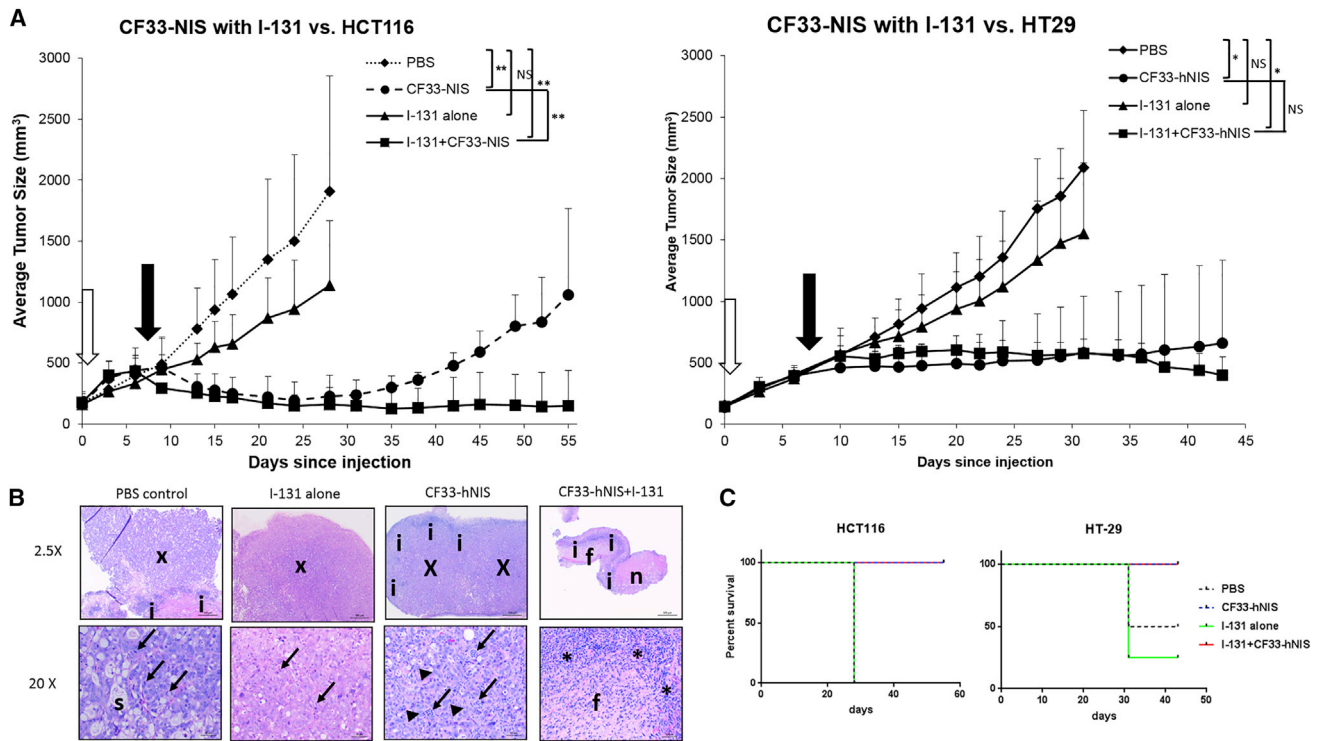


Figure 6. I-131 Intravenous Synergy with CF33-hNIS versus HT29 and HCT116 Colon Cancer Cells

(A) Flank xenografts were created in nude mice with 2×10^6 cells in HCT116 xenografts and 3×10^6 cells in HT29 xenografts. Ten days later, when tumors reached average volume of 150 mm^3 , they were randomized to four treatment groups: (1) PBS control, (2) I-131 alone, (3) CF33-hNIS alone (1×10^4 pfu), and (4) I-131 + CF33-hNIS (1×10^4 pfu). I-131 injection was intravenous, whereas viral injection was intratumoral. In the combination group, I-131 injection occurred 7 days after viral infection. First arrow (white) represent virus delivery, and second arrow (black) represents I-131 for combination group. In I-131-alone group, radioisotope is administered on same day as virus. (B) Tumors from mice with HT29 xenografts. PBS and I-131 are composed almost entirely of xenograft cells (x; upper panels for these mice). A small zone of inflammation is present adjacent to the xenograft cells in mouse PBS, although few, if any, inflammatory cells are found in the tumor from mouse I-131. Mitotic figures (arrows) are common in xenograft cells in tumors from these mice (lower panels), and secretory material(s) is seen in the tumor from mouse PBS. The tumor from mouse CF33-hNIS (upper panel for this mouse) has a large area composed of xenograft cells (x) that is surrounded by a thick rim of inflammation (i). A higher magnification photograph of this tumor (lower panel for this mouse) shows that small clusters of xenograft cells (arrowheads) are surrounded by an abundant inflammatory cell infiltrate that has a prominent component of neutrophils (arrows). The tumor from mouse CF33-hNIS + I-131 (upper panel for this mouse) lacks xenograft cells and is instead composed of areas of necrosis (n), inflammation (i), and fibrosis (f). The lower panel shows the inflammatory cell infiltrate (i) and fibrosis (f) at higher magnification. H&E stain is shown. (C) Survival curves demonstrating mouse survival in each group. In HCT116 mice, all four in the PBS and I-131-alone groups were euthanized at 28 days upon reaching predetermined size endpoints. All others were alive at 55 days. In HT29 mice, two mice in the PBS group and three in the I-131-alone group were euthanized secondary to reaching predetermined size endpoints. All other mice were euthanized at day 43. NIS, sodium iodide symporter. * $p < 0.05$, ** $p < 0.0001$.

refine imaging techniques, to confirm deep tissue imaging in orthotopic and metastatic models, and to delineate comparisons of SPECT with PET. It will be interesting to investigate in future experiments whether radioiodine uptake correlates to viral tumor titer throughout all time points and to further refine imaging techniques and timing, using immunocompetent and orthotopic or metastatic models.

Conclusions

In summary, our novel chimeric orthopoxvirus CF33-hNIS encodes a functional sodium iodide symporter, induces caspase-independent ICD, allows real-time noninvasive imaging of viral infection, and most importantly, kills colorectal cancer *in vitro* and *in vivo*. Our present study showed that CF33-hNIS synergizes with I-131. Most notably, this vector can be tracked in real time and used in concert

with radioisotope therapy in order to maximize the reach of CF33-hNIS or similar vectors while minimizing dose. We anticipate that this would decrease toxicity and cost while maximizing tumoricidal activity and allowing for tracking of viral replication and efficacy.

MATERIALS AND METHODS

Cell Lines and Maintenance

For standard viral plaque assays, African green monkey kidney fibroblasts (CV-1), purchased from the American Type Culture Collection (ATCC, Manassas, VA, USA), were cultured at 37°C with 5% CO_2 in DMEM (Corning, Corning, NY, USA). Human colorectal cell lines were all purchased from ATCC. HCT-116 and HT-29s were maintained in McCoy's 5A medium (ATCC, Manassas, VA, USA) per ATCC instructions. All cells were kept at 37°C and 5% CO_2 . Unless

stated otherwise, cells were supplemented with 10% fetal bovine serum (FBS) and 1% antibiotic-antimycotic solution, both purchased from Corning (Corning, NY, USA). Cell lines were expanded and frozen down after a maximum of three passages. Efforts were made to ensure all experiments took place after less than 10 passages.

CF33 Chimerization and hNIS Cloning

The chimerization process of the CF33 backbone virus has been described in previous publications.^{14,15} In brief, nine strains of orthopoxvirus were used to create CF33 by co-infecting CV-1 cells and fostering chimerization. These included cowpox, raccoonpox, rabbitpox, and multiple vaccinia virus strains, all purchased from ATCC and grown and titrated in CV-1 cells. Following the co-infection, 100 individual plaques were chosen and then thrice purified in CV-1 cells to obtain 100 clonally purified chimeric orthopoxviruses. High-throughput screening was used to compare the cytotoxic efficacy of chimeric clones with each other and with parental strains versus the NCI-60 panel of human cancer cell lines. CF33 was selected as the chimeric isolate that demonstrated superior cell killing in the NCI-60 panel compared with all parental viruses and other plaque-purified isolates.

To generate CF33 expressing hNIS, the hNIS expression cassette under control of the vaccinia virus H5 synthetic early (SE) promoter was cloned using Sac I and BamHI restriction sites and was inserted at the thymidine kinase locus of CF33¹⁶ with transient dominant selection as previously described using the guanine phosphoribosyltransferase marker, as has been similarly described with insertion of firefly luciferase.^{15,37}

Immunofluorescence

In order to examine vaccinia and hNIS co-expression, HT29 and HCT116 cells infected with CF33-hNIS at MOI 0.01 were compared with non-infected controls. Cells were fixed with 4% paraformaldehyde at room temperature for 15 min, permeabilized with 0.1% Triton X-100 in PBS for 5 min on ice, and blocked for 30 min at 37°C in Tris-NaCl-blocking buffer (0.1 M Tris-HCl, pH 7.5, 0.15 NaCl, and 0.5% Blocking Reagent; category number FP1020; PerkinElmer). After blocking, cells were incubated with anti-sodium iodide symporter antibody (ab17795; Abcam) at 1:50 dilution in Tris-NaCl-blocking buffer and incubated with a secondary Alexa Fluor 488-conjugated goat anti-mouse immunoglobulin G (IgG) H&L (ab150113; Abcam) at 1:100 dilution. Cells were re-blocked in Tris-NaCl-blocking buffer and stained with anti-vaccinia virus antibody (ab35219; Abcam) at 1:200 dilution and a secondary Alexa Fluor 594-conjugated goat anti-Rabbit IgG H&L (ab150080; Abcam) at 1:100 dilution to document surface expression of NIS on virally infected cells.

Cytotoxicity Assay

Human colorectal cancer cell lines HCT-116 and HT29 were plated at 3×10^3 cells per well in cell-specific media supplemented with 5% FBS and 1% antibiotic-antimycotic solution in 96-well flat-bottom plates. The following day, cells were infected with virus at MOIs 1 and 0.01.

For the next 5 days, cell survival was determined by comparing absorption of infected cells with uninfected cells after 3-h incubation with CellTiter 96 AQueous One Solution Cell Proliferation Assay per manufacturer's protocol (Promega, Madison, WI, USA).

Viral Growth Assays

A total of 5×10^5 of HCT-116 and HT-29 cells were seeded in six-well plates. The following day, cells were counted and infected at an MOI of 0.01 PFU per cell with CF33-hNIS and CF33-GFP in a total volume of 0.5 mL medium containing 2.5% FBS. After 1 h, the inoculum was aspirated and fresh medium was added to each well, and plates were returned to the incubator. At the indicated times, cells were scraped into the medium and subjected to three rounds of freeze-thaw to ensure complete cell lysis and virus release. Viral titers in the lysates were determined by standard plaque assay. Lysates were serially diluted and used to infect 24-well plates of CV-1 cells. One hour after infection, 1 mL of medium containing 1% methyl-cellulose was added to each well. Forty-eight hours post-infection, 250 μ L 0.5% (w/v) crystal violet was added to each well, and the plates were left at room temperature overnight. The next day, the plates were washed and plaques were counted.

Cell Death Analysis

Apoptosis Assays

Flow Cytometry. For Annexin V, caspase-3, or PI staining, cells were infected with CF33-NIS at an MOI of 5 in 3 mL of medium supplemented with 2.5% FBS. After 1-h incubation, cells were washed twice with PBS before addition of complete growth medium. Cells were then harvested at 18 and 48 h and stained with Annexin V, propidium iodide, or caspase-3 antibody per manufacturer's instructions (FITC Annexin V/Dead cell apoptosis kit, category no. V13242 [Invitrogen]; Live/Dead Fixable far red dead cell stain kit, category no. L34973; PE Active Caspase-3 Apoptosis kit, category no. 550914 [BD Pharmingen]). Stained cells were then analyzed on a BD Accuri C6 Flow Cytometer (BD Biosciences).

TUNEL Assay. Cells were plated at 2×10^5 cells/well in an eight-well chamber slide (category no. 154534; Thermo Fisher Scientific). The following day, cells were infected with CF33-hNIS at MOI 0.01 pfu/cell. After 18 or 48 h of infection, TUNEL reaction was performed using *In Situ* Cell Death Detection kit (Roche; category no. 11684795910) following the manufacturer's instructions; then cells were blocked in Tris-NaCl-blocking buffer, and stained with anti-vaccinia virus antibody (ab35219; Abcam) and a secondary Alexa Fluor 594-conjugated goat anti-Rabbit IgG H&L (ab150080; Abcam).

ICD Assays

Three independent assays were used to monitor ICD: ATP level assay, flow cytometric assessment of calreticulin levels, and detection of HMGB1 release.

Secretion of ATP. Cells were infected at MOI 5 and were incubated for 16 h. After incubation, supernatants were collected, ATP levels were determined according to the manufacturer's instructions (ATP

Determination Kit, category no. A22066; Invitrogen), and luminescence was measured with a TECAN microplate reader (Life Sciences).

Calreticulin. Cells were infected with CF33-hNIS (MOI 5) for 16 h. 1×10^6 cells were resuspended in PBS with 2% FBS and stained with isotype control (EPR25A; Abcam) or anti-calreticulin antibody (EPR3924; Abcam). After staining, FACS analysis was performed.

HMGB1. Cells were infected with CF33-hNIS (MOI 5). Supernatants were collected at different time points and concentrated using a column with 10-kDa size cutoff. The concentrated supernatants were loaded (15 μ L/well) for western blotting. HMGB1 was detected using a rabbit anti-HMGB1 antibody (category no. ab18256; Abcam) at 1:100 dilution followed by an HRP-labeled goat anti-rabbit secondary antibody (category no. ab205718; Abcam) at 1:5,000 dilution.

In Vivo Studies

Animal studies were performed under the City of Hope Institutional Animal Care and Use Committee (IACUC)-approved protocol.

Establishment of Colorectal Cancer Flank Xenografts

Six-week-old Hsd:Athymic Nude-*Foxn1*tm female mice (Envigo, Indianapolis, IN, USA) were purchased and acclimatized for 1 week. Bilateral flank tumors were generated by injecting $2-5 \times 10^6$ HCT116 or HT29 cells in a total of 100 μ L PBS containing 50% matrigel for each tumor. When average tumor size approached 150 mm³, mice were divided into experimental groups.

In Vivo Efficacy of CF33-hNIS

Mice were divided into the following groups (n = at least 4 mice per group): PBS control HT29, PBS control HCT116, CF33-hNIS HT29, and CF33-hNIS HCT116. When tumors reached average volume of 150 mm³, mice were treated with 10^5 PFU of CF33-NIS or PBS, and experiments were also repeated at 10^4 PFU. In all groups, tumor volume was measured twice weekly with tumor volume V (mm³) = $(1/2) \times A^2 \times B$, where A is the shortest and B is the longest measurement. Percent tumor change was calculated based upon initial tumor size at time of intervention. At the time of euthanasia, tumors and solid organs were harvested. Tissues were split into halves formalin-fixed for immunohistochemical analysis. Two mice from each group were sacrificed at day 10 following viral injection. The remaining mice were euthanized on day 50.

In Vivo I-124 Uptake Measured by PET/CT

Mice were divided into imaging and control groups (n = 4 mice). To analyze tumor imageability after intratumoral delivery, mice received an intratumoral injection of 10^4 PFU per tumor of either CF33-hNIS, CF33-Fluc, or PBS when tumors reached 100 mm³. At 7, 15, and 22 days post-viral infection, mice in each group received 200 μ Ci of I-124 injected per tail vein. The radioisotope was obtained from the City of Hope Small Animal Imaging Core Radiopharmacy. PET imaging was then obtained 2 h following injection using the small-animal PET scanner (microPET R4; Siemens Corporation), which provides fully three-dimensional PET imaging with spatial resolution

of better than 2.0 mm and quantitative accuracy for measurement of tissue activity concentration on the order of 10%. The 8-cm axial field of view is adequate for simultaneous whole-body imaging of mice. Advanced image reconstruction software provides resolution approaching 1.0 mm. Quantitative accuracy is supported by scatter, dead time, and measured attenuation corrections. The system includes a fully developed image analysis package that supports volumetric regions of interest and fusion of PET with co-registered anatomic CT. In order to protect mouse thyroids from radioiodine ablation, all mice received T4 supplementation with 5 mg levothyroxine/L of water beginning 1 week prior to radioiodine administration.

In Vivo Combination Therapy of CF33-hNIS and I-131

Bilateral flank xenografts were implanted in athymic nude female mice using 3×10^6 HT29 cells in 100 μ L of PBS containing 50% matrigel. Ten days later, when tumors reached average volume of 150 mm³, they were randomized to four treatment groups: PBS control, i.v. I-131 alone, intratumoral CF33-hNIS alone, or combination of i.v. I-131 with intratumor (i.t.) CF33-hNIS. I-131 injection was i.v., whereas viral injection was intratumoral. In the combination group, I-131 injection occurred 7 days after viral infection. Doses of 1×10^4 PFU of i.t. CF33-NIS were used at day zero in both groups using virus. In the radioisotope alone group, I-131 was administered on the same date as virus. Based upon previous publications exploring radioisotope synergy, a dose of 2.5 mCi of I-131 was chosen for initial experiments using HT29.^{13,31} Dose of CF33-hNIS was 1×10^4 PFU delivered only to the right flank tumor in order to assess whether synergy could also be seen in uninjected tumors. In subsequent experiments using HCT116 unilateral xenografts created as above, I-131 dose was reduced to 2.0 mCi. As above, in order to protect mouse thyroids from radioiodine ablation, all mice received T4 supplementation with 5 mg levothyroxine/L of water beginning 1 week prior to radioiodine administration.

Immunohistochemistry

Tumors harvested at euthanasia were formalin fixed for 2 weeks, embedded in paraffin, and cut into 5- μ m-thick sections. H&E staining was done for routine histopathological examination. Slides were deparaffinized and applied for heat-mediated antigen retrieval per manufacturer's protocol (IHC World, Ellicott City, MD, USA). Tumor sections were then permeabilized with methanol, and Tris-NaCl-blocking buffer (PerkinElmer, Waltham, MA, USA) was used to decrease background for 20 min. Rabbit anti-vaccinia virus antibody 1:200 in Tris-NaCl-blocking buffer (category no. ab35219; Abcam, Cambridge, MA, USA) was added overnight in a humidified chamber at 4°C. The next day, tumor sections were secondarily stained with Alexa Fluor 488-conjugated goat anti-rabbit (category no. ab150080; Abcam, Cambridge, MA, USA) for 1 h at room temperature. Finally, DAPI was added for nuclear staining, and images were obtained using EVOS FL Auto Imaging System (Thermo Fisher Scientific, Waltham, MA, USA).

Statistical Analysis

Statistical analysis was performed using GraphPad Prism (Version 7.01, La Jolla, CA, USA). Student's t test or one-way ANOVA was

used to evaluate for statistical significance. $p < 0.05$ was considered significant.

SUPPLEMENTAL INFORMATION

Supplemental Information can be found online at <https://doi.org/10.1016/j.omto.2019.04.001>.

AUTHOR CONTRIBUTIONS

S.G.W. conceptualized and directly supervised projects, drafted the manuscript, and refined figures. S.-I.K., S.C., M.P.O., J.L., and V.S. assisted with conceptualization of experiments, performed experiments, and revised and edited the manuscript. N.G.C. designed and constructed the viruses. J.L. helped with generation and production of the viruses. S.-I.K. kept raw data and created many raw figures. Y.W., N.G.C., and Y.F. assisted with conceptualization of the project, assisted with direction of experiments, and revised and edited the manuscript.

CONFLICTS OF INTEREST

The authors declare no competing interests.

ACKNOWLEDGMENTS

The authors are very grateful to Junie Chea and the City of Hope Small Animal Imaging Core for their assistance with radioisotope injections and imaging. S.G.W.'s work is supported by American Cancer Society Mentored Research Scholar Grant MRSR-16-047-01-MPC. The authors are grateful to Dr. Indra M. Newman for her scientific editorial expertise.

REFERENCES

- Siegel, R.L., Miller, K.D., and Jemal, A. (2018). Cancer statistics, 2018. *CA Cancer J. Clin.* 68, 7–30.
- van der Geest, L.G., Lam-Boer, J., Koopman, M., Verhoef, C., Elferink, M.A., and de Wilt, J.H. (2015). Nationwide trends in incidence, treatment and survival of colorectal cancer patients with synchronous metastases. *Clin. Exp. Metastasis* 32, 457–465.
- Riihimäki, M., Hemminki, A., Sundquist, J., and Hemminki, K. (2016). Patterns of metastasis in colon and rectal cancer. *Sci. Rep.* 6, 29765.
- Kaufman, H.L., Amatruda, T., Reid, T., Gonzalez, R., Glaspy, J., Whitman, E., Harrington, K., Nemunaitis, J., Zloza, A., Wolf, M., and Senzer, N.N. (2016). Systemic versus local responses in melanoma patients treated with talimogene laherparepvec from a multi-institutional phase II study. *J. Immunother. Cancer* 4, 12.
- Davis, J.J., and Fang, B. (2005). Oncolytic virotherapy for cancer treatment: challenges and solutions. *J. Gene Med.* 7, 1380–1389.
- Warner, S.G., O'Leary, M.P., and Fong, Y. (2017). Therapeutic oncolytic viruses: clinical advances and future directions. *Curr. Opin. Oncol.* 29, 359–365.
- Russell, S.J., Peng, K.W., and Bell, J.C. (2012). Oncolytic virotherapy. *Nat. Biotechnol.* 30, 658–670.
- Lauer, U.M., Schell, M., Beil, J., Berchtold, S., Koppenhöfer, U., Glatzle, J., Königsrainer, A., Möhle, R., Nann, D., Fend, F., et al. (2018). Phase I Study of Oncolytic Vaccinia Virus GL-ONC1 in Patients with Peritoneal Carcinomatosis. *Clin. Cancer Res.* 24, 4388–4398.
- Abou-Alfa, G.K., Galle, P.R., Chao, Y., Brown, K.T., Heo, J., Borad, M.J., Luca, A., Pelusio, A., Agathon, D., Lusky, M., et al. (2016). PHOCUS: a phase 3 randomized, open-label study comparing the oncolytic immunotherapy Pexa-Vec followed by sorafenib (SOR) vs SOR in patients with advanced hepatocellular carcinoma (HCC) without prior systemic therapy. *J. Clin. Oncol* 34 (Suppl 15), TPS4146.

- Bennett, J.J., Tjuvajev, J., Johnson, P., Doubrovin, M., Akhurst, T., Malholtra, S., Hackman, T., Balatoni, J., Finn, R., Larson, S.M., et al. (2001). Positron emission tomography imaging for herpes virus infection: Implications for oncolytic viral treatments of cancer. *Nat. Med.* 7, 859–863.
- Miller, A., and Russell, S.J. (2016). The use of the NIS reporter gene for optimizing oncolytic virotherapy. *Expert Opin. Biol. Ther.* 16, 15–32.
- Haddad, D., Chen, C.H., Carlin, S., Silberhumer, G., Chen, N.G., Zhang, Q., Longo, V., Carpenter, S.G., Mitra, A., Carson, J., et al. (2012). Imaging characteristics, tissue distribution, and spread of a novel oncolytic vaccinia virus carrying the human sodium iodide symporter. *PLoS ONE* 7, e41647.
- Gholami, S., Chen, C.H., Lou, E., Belin, L.J., Fujisawa, S., Longo, V.A., Chen, N.G., Gönen, M., Zanzonico, P.B., Szalay, A.A., and Fong, Y. (2014). Vaccinia virus GLV-1h153 in combination with 131I shows increased efficiency in treating triple-negative breast cancer. *FASEB J.* 28, 676–682.
- O'Leary, M.P., Warner, S.G., Kim, S.-I., Chaurasiya, S., Lu, J., Choi, A.H., Park, A.K., Woo, Y., Fong, Y., and Chen, N.G. (2018). A Novel Oncolytic Chimeric Orthopoxvirus Encoding Luciferase Enables Real-Time View of Colorectal Cancer Cell Infection. *Mol. Ther. Oncolytics* 9, 13–21.
- O'Leary, M.P., Choi, A.H., Kim, S.I., Chaurasiya, S., Lu, J., Park, A.K., Woo, Y., Warner, S.G., Fong, Y., and Chen, N.G. (2018). Novel oncolytic chimeric orthopoxvirus causes regression of pancreatic cancer xenografts and exhibits abscopal effect at a single low dose. *J. Transl. Med.* 16, 110.
- Choi, A.H., O'Leary, M.P., Lu, J., Kim, S.I., Fong, Y., and Chen, N.G. (2018). Endogenous Akt Activity Promotes Virus Entry and Predicts Efficacy of Novel Chimeric Orthopoxvirus in Triple-Negative Breast Cancer. *Mol. Ther. Oncolytics* 9, 22–29.
- Galluzzi, L., Vitale, I., Aaronson, S.A., Abrams, J.M., Adam, D., Agostinis, P., Alnemri, E.S., Altucci, L., Amelio, I., Andrews, D.W., et al. (2018). Molecular mechanisms of cell death: recommendations of the Nomenclature Committee on Cell Death 2018. *Cell Death Differ.* 25, 486–541.
- Guo, Z.S., and Bartlett, D.L. (2004). Vaccinia as a vector for gene delivery. *Expert Opin. Biol. Ther.* 4, 901–917.
- Worschech, A., Chen, N., Yu, Y.A., Zhang, Q., Pos, Z., Weibel, S., Raab, V., Sabatino, M., Monaco, A., Liu, H., et al. (2009). Systemic treatment of xenografts with vaccinia virus GLV-1h68 reveals the immunologic facet of oncolytic therapy. *BMC Immunomics* 10, 301.
- Spitzweg, C., and Morris, J.C. (2002). The sodium iodide symporter: its pathophysiological and therapeutic implications. *Clin. Endocrinol. (Oxf.)* 57, 559–574.
- Dingli, D., Russell, S.J., and Morris, J.C., 3rd (2003). In vivo imaging and tumor therapy with the sodium iodide symporter. *J. Cell. Biochem.* 90, 1079–1086.
- Groot-Wassink, T., Aboagye, E.O., Wang, Y., Lemoine, N.R., Reader, A.J., and Vassaux, G. (2004). Quantitative imaging of Na/I symporter transgene expression using positron emission tomography in the living animal. *Mol. Ther.* 9, 436–442.
- Willhauck, M.J., Sharif Samani, B.R., Gildehaus, F.J., Wolf, I., Senekowitsch-Schmidtke, R., Stark, H.J., Göke, B., Morris, J.C., and Spitzweg, C. (2007). Application of 188rhenium as an alternative radionuclide for treatment of prostate cancer after tumor-specific sodium iodide symporter gene expression. *J. Clin. Endocrinol. Metab.* 92, 4451–4458.
- Klutzb, K., Willhauck, M.J., Wunderlich, N., Zach, C., Anton, M., Senekowitsch-Schmidtke, R., Göke, B., and Spitzweg, C. (2011). Sodium iodide symporter (NIS)-mediated radionuclide ((131)I, (188)Re) therapy of liver cancer after transcriptionally targeted intratumoral in vivo NIS gene delivery. *Hum. Gene Ther.* 22, 1403–1412.
- Heinrich, B., Klein, J., Delic, M., Goepfert, K., Engel, V., Geberzahn, L., Lusky, M., Erbs, P., Preville, X., and Moehler, M. (2017). Immunogenicity of oncolytic vaccinia viruses JX-GFP and TG6002 in a human melanoma in vitro model: studying immunogenic cell death, dendritic cell maturation and interaction with cytotoxic T lymphocytes. *Oncotargets Ther.* 10, 2389–2401.
- Veyer, D.L., Carrara, G., Maluquer de Motes, C., and Smith, G.L. (2017). Vaccinia virus evasion of regulated cell death. *Immunol. Lett.* 186, 68–80.
- Haddad, D., Chen, N.G., Zhang, Q., Chen, C.H., Yu, Y.A., Gonzalez, L., Carpenter, S.G., Carson, J., Au, J., Mitra, A., et al. (2011). Insertion of the human sodium iodide symporter to facilitate deep tissue imaging does not alter oncolytic or replication capability of a novel vaccinia virus. *J. Transl. Med.* 9, 36.

28. Chen, R.F., Li, Z.H., Pan, Q.H., Zhou, J.J., Tang, Q.B., Yu, F.Y., Zhou, Q.B., Wang, J., and Chen, J.S. (2007). In vivo radioiodide imaging and treatment of pancreatic cancer xenografts after MUC1 promoter-driven expression of the human sodium-iodide symporter. *Pancreatology* 7, 505–513.
29. Penheiter, A.R., Wegman, T.R., Classic, K.L., Dingli, D., Bender, C.E., Russell, S.J., and Carlson, S.K. (2010). Sodium iodide symporter (NIS)-mediated radiovirotherapy for pancreatic cancer. *AJR Am. J. Roentgenol.* 195, 341–349.
30. Haddad, D., Chen, N., Zhang, Q., Chen, C.H., Yu, Y.A., Gonzalez, L., Aguilar, J., Li, P., Wong, J., Szalay, A.A., and Fong, Y. (2012). A novel genetically modified oncolytic vaccinia virus in experimental models is effective against a wide range of human cancers. *Ann. Surg. Oncol.* 19 (Suppl 3), S665–S674.
31. Haddad, D., Zanzonico, P.B., Carlin, S., Chen, C.H., Chen, N.G., Zhang, Q., Yu, Y.A., Longo, V., Mojica, K., Aguilar, R.J., et al. (2012). A vaccinia virus encoding the human sodium iodide symporter facilitates long-term image monitoring of virotherapy and targeted radiotherapy of pancreatic cancer. *J. Nucl. Med.* 53, 1933–1942.
32. Mansfield, D.C., Kyula, J.N., Rosenfelder, N., Chao-Chu, J., Kramer-Marek, G., Khan, A.A., Roulstone, V., McLaughlin, M., Melcher, A.A., Vile, R.G., et al. (2016). Oncolytic vaccinia virus as a vector for therapeutic sodium iodide symporter gene therapy in prostate cancer. *Gene Ther.* 23, 357–368.
33. Workenhe, S.T., and Mossman, K.L. (2014). Oncolytic virotherapy and immunogenic cancer cell death: sharpening the sword for improved cancer treatment strategies. *Mol. Ther.* 22, 251–256.
34. Whilding, L.M., Archibald, K.M., Kulbe, H., Balkwill, F.R., Öberg, D., and McNeish, I.A. (2013). Vaccinia virus induces programmed necrosis in ovarian cancer cells. *Mol. Ther.* 21, 2074–2086.
35. Guo, Z.S., Liu, Z., and Bartlett, D.L. (2014). Oncolytic Immunotherapy: Dying the Right Way is a Key to Eliciting Potent Antitumor Immunity. *Front. Oncol.* 4, 74.
36. Breitbach, C.J., Paterson, J.M., Lemay, C.G., Falls, T.J., McGuire, A., Parato, K.A., Stojdl, D.F., Daneshmand, M., Speth, K., Kirn, D., et al. (2007). Targeted inflammation during oncolytic virus therapy severely compromises tumor blood flow. *Mol. Ther.* 15, 1686–1693.
37. Falkner, F.G., and Moss, B. (1990). Transient dominant selection of recombinant vaccinia viruses. *J. Virol.* 64, 3108–3111.